Self-Assembly of Flexible−Semiflexible−Flexible Triblock Copolymers

ARTICLE *in* MACROMOLECULES · JUNE 2014

Impact Factor: 5.8 · DOI: 10.1021/ma500798z

Macromolecules

Article

pubs.acs.org/Macromolecules

Self-Assembly of Flexible−Semiflexible−Flexible Triblock Copolymers

Maito Koga,[†] Kohei Abe,[†] Kazunori Sato,[†] Jun Koki,[‡] Sungmin Kang,[†] Koichi Sakajiri,[†] Junji Watanabe,[†] and Masatoshi Tokita*,[†]

[†]Department of Organic and Polymeric Materials and [‡]Technical Department, Tokyo Institute of Technology, Ookayama, Meguro-ku, Tokyo 152-8552, Japan

ABSTRACT: The self-assembly of ABA triblock copolymers comprising flexible amorphous poly(ethyl methacrylate) (PEMA, A block) and semiflexible liquid crystal (LC) polyester (B block) was investigated for amorphous block volume fractions (φ) ranging from 20% to 80%. Two copolymer series with different LC block molecular weights ($M_{n,LC}$) were examined. At φ < 55%, block copolymers with $M_{n,LC}$ = 11 600 formed lamellar microdomains in which LC segments mostly extended along the lamella normal but folded to fit in the lamellae. When φ was augmented, the LC segment fold (N_{fold}) increased to enhance the interface between the LC and amorphous segments and counterbalanced the increase in amorphous lamella thickness by reducing the LC lamella thickness. When φ > 68%, the LC lamellae were divided into cubes, transforming into spheres in the PEMA matrix. When $M_{n,LC}$ decreased to 6300, the copolymers showed similar morphology. However, the lamellae adopted zigzag configurations showing a greater tilting angle between the lamella normal to the LC chain axis with increasing φ. Thus, the LC and PEMA segments enhanced their interface by mutually sliding along the chain axis instead of increasing N_{fold}.

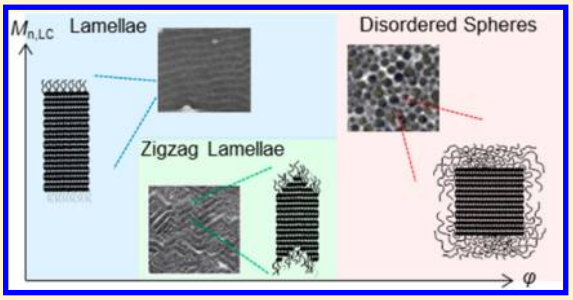

1. INTRODUCTION

Block copolymers are expected to play a crucial role in nanolithography, nanopatterning, and templating applications because their self-assembly generates nanostructures with specific orientational order.[1] The fundamental phase behaviors and self-assembly are well-understood for block copolymers comprising flexible segments or coils. These copolymers typically form spherical, cylindrical, and lamellar microdomains depending on the segment volume fractions.[2] Although many applications may result from the incorporation of various functional segments into block copolymers and nanostructures, most of these segments exhibit rodlike shapes. For example, semiconducting polymers and biopolymers exhibit rigid rodlike conformations originating from their π-conjugated polymer backbones and helical secondary structures, respectively. Therefore, the incorporation of functional segments into block copolymers produces flexible−rod copolymers.[3] Flexible−rod copolymers form characteristic morphologies due to the orientational order of the rod blocks and the conformational asymmetry between the rodlike and coil blocks. Rod segments are accommodated into wavy, zigzag, and perforated lamellae, strips, and pucks.[4−8]

The morphology of flexible−semiflexible−flexible triblock copolymers has recently been investigated.[9−12] The central semiflexible block was a main-chain liquid crystal (LC) polymer composed of alternately connected rigid aromatic mesogens and flexible alkyl spacers. Both ends of this LC polymer were tethered to flexible segments. These copolymers with a smectic LC central block formed lamellar microdomains when the volume fraction of amorphous segments (φ) ranged from 20% to 52%.[9] In these microdomains, smectic layers appeared parallel to the lamellae, indicating that the LC segments mainly adopted an extended conformation perpendicular to the interface. However, the contour length of the LC segments (50 nm) was much larger than the LC lamella thickness (d_{LC} = 10−14 nm), suggesting that the LC segments were folded to fit in the lamellae. When the molecular weight of the amorphous segment ($M_{n,am}$) increased, d_{LC} decreased, thus counteracting the increase in amorphous lamella thickness (d_{am}). As a result of this decrease, the lamellar spacing (d_0) remained almost constant despite rising copolymer molecular weights. This indicates that the semiflexible segment increases the number of folds (N_{fold}) to enlarge the interface with the amorphous segment with increasing $M_{n,am}$.

In this study, the self-assembly of flexible−semiflexible−flexible block copolymers was examined for a wider φ range (16%−85%). The investigated copolymers were poly(ethyl methacrylate)-*block*-BB-3(2-Me)-*block*-poly(ethyl methacrylate), in which the central polyester block BB-3(2-Me) comprised 4,4′-biphenyl dicarboxylic acid and 2-methyl-1,3-propanediol (Chart 1). Two series of copolymers were prepared using two BB-3(2-Me) polyesters with molecular weights ($M_{n,LC}$) of 11 600 and 6300. The copolymers are identified as BB-3(2-Me)-*x*-φ, where *x* corresponds to $M_{n,LC}$

Received: April 16, 2014
Revised: June 6, 2014
Published: June 20, 2014

Chart 1

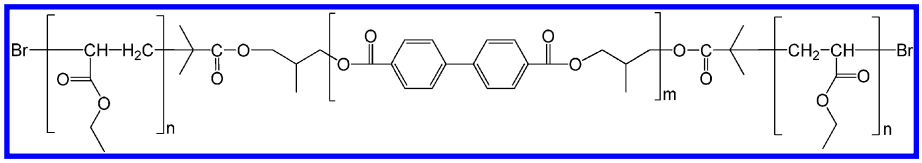

divided by 100 and φ represents the poly(ethyl methacrylate) (PEMA) segment volume percentage. BB-3(2-Me)-116-φ copolymers formed lamellar microdomains for φ < 55%. For φ > 68%, LC segments formed discrete spheres. BB-3(2-Me)-63-φ copolymers exhibited a similar morphological dependence on φ. However, the lamellae displayed zigzag configurations that exhibited increased tilt angles with increasing φ. This zigzag lamellar morphology is a characteristic of flexible−rod block copolymers, which indicates that short semiflexible segments can behave as rigid rods.

2. EXPERIMENTAL SECTION

2.1. Materials. BB-3(2-Me)-*x*-φ block copolymers were synthesized as previously reported.[9,10] Hydroxyl-terminated BB-3(2-Me) polyesters were prepared by the melt transesterification of dimethyl 4,4′-bibenzoate and excess 2-methyl-1,3-propanediol in the presence of the isopropyl titanate catalyst at 240 °C. The reaction of the hydroxyl-terminated polyester with 2-bromoisobutylate bromide produced the telechelic α,ω-di-2-bromoisobutyrate BB-3(2-Me) polyester, which served as a macroinitiator for the copper(I)-catalyzed atom-transfer radical polymerization of ethyl methacrylate at 60−80 °C using anisole as a solvent to yield polydisperse yet unimodal block copolymers. The values of $M_{n,LC}$ and $M_{n,am}$ were determined by ^{1}H NMR spectroscopy, and the polydispersity indices of the copolymers (M_w/M_n) were obtained by size-exclusion chromatography (SEC) (Table 1). φ values were calculated from $M_{n,LC}$, $M_{n,am}$, and the densities of the segments (ρ_{LC} = 1.27 g cm^{-3}, ρ_{am} = 1.12 g cm^{-3}).

Table 1. Characterization of Polymers

sample	$M_{n,LC}$ [a]	$M_{n,PEMA}$ [a]	M_w/M_n [b]
OH-terminated BB-3(2-Me)-116	11600	–	2.11
BB-3(2-Me)-116-85	11600	56700	1.82
BB-3(2-Me)-116-73	11600	27900	1.81
BB-3(2-Me)-116-50	11600	10300	1.94
BB-3(2-Me)-116-42	11600	7500	1.75
BB-3(2-Me)-116-39	11600	6400	1.75
BB-3(2-Me)-116-23	11600	3200	1.71
OH-terminated BB-3(2-Me)-63	6300	–	2.11
BB-3(2-Me)-63-68	6300	11800	1.48
BB-3(2-Me)-63-62	6300	9200	1.81
BB-3(2-Me)-63-52	6300	5900	1.49
BB-3(2-Me)-63-45	6300	4600	1.50
BB-3(2-Me)-63-36	6300	3100	1.46
BB-3(2-Me)-63-28	6300	2100	1.59
BB-3(2-Me)-63-16	6300	1000	1.62

[a]Determined by ^{1}H NMR spectroscopy. [b]Determined by SEC.

2.2. Methods. Differential scanning calorimetry (DSC) measurements were performed using a PerkinElmer Pyris 1 differential scanning calorimeter equipped with an Intracooler II under a flow of dry nitrogen. Wide-angle X-ray scattering (WAXS) patterns were measured using a Bruker D8 DISCOVER diffractometer equipped with a Vantec-500 detector, and small-angle X-ray scattering (SAXS) patterns were acquired on a Bruker NanoSTAR-U system using Cu Kα radiation. Transmission electron microscopy (TEM) was performed using a Hitachi H-7650 Zero A electron microscope operating at 100 kV in bright-field mode. Samples were exposed to RuO_4 vapors at ambient temperature to selectively stain the LC domains and then microtomed into ultrathin sections. Densities were measured by the sink−float method at 20 °C in an aqueous potassium bromide solution whose density was determined pycnometrically.

3. RESULTS

3.1. Phase Diagram of LC Block Copolymers. The microdomain morphologies of BB-3(2-Me)-*x*-φ copolymers determined by SAXS and TEM were combined to develop a phase diagram (Figure 1). In this diagram, the lines represent

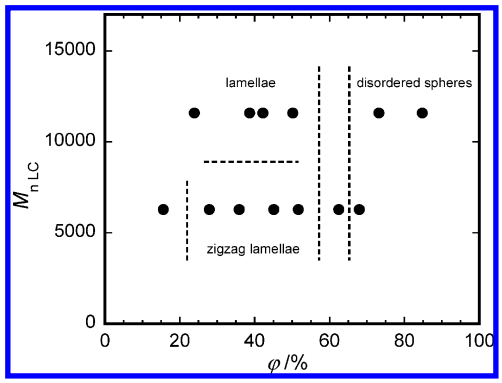

Figure 1. Morphological phase diagram for BB-3(2-Me)-*x*-φ copolymers.

phase behaviors based on experimental data and may be used to delineate general trends in the copolymer phase behavior. At low φ, neither PEMA cylinders nor spheres were observed in the LC matrix. Instead, lamellar morphologies were observed for φ < 55%. On the other hand, the LC segments formed disordered spheres in an amorphous matrix for φ > 68%. Spheres and lamellae coexisted in the copolymers for φ values ranging between 55% and 68%. Zigzag lamellae were formed for φ values ranging between 20% and 50%, which is a characteristic of BB-3(2-Me)-63-φ copolymers with a short LC segment.

3.2. Smectic LC Structure in the Copolymers. The BB-3(2-Me) segments in the copolymers formed isotropic liquid and smectic CA (SmCA) phases with decreasing temperature. The smectic LC phase did not crystallize and vitrified on cooling at usual rates as low as 1 °C min^{-1}. DSC thermograms measured at a heating rate of 10 °C min^{-1} exhibited a step in the heat capacity at ca. 60 °C and an endothermic peak corresponding to the isotropization of the SmCA LC. Thus, although BB-3(2-Me) segments were segregated from PEMA segments, the copolymers exhibited a single glass transition because the BB-3(2-Me) and PEMA segments presented similar glass transition temperatures (T_g). The temperature of the endothermic peak ranged from 145 to 172 °C depending on $M_{n,LC}$ and φ. Table 2 lists the T_g values as well as isotropization temperatures (T_i) and enthalpies (ΔH_i).

Fibrous samples were spun from isotropic melts at 180 °C and annealed at a temperature of (T_i − 15 °C) for 12 h before

dx.doi.org/10.1021/ma500798z | Macromolecules 2014, 47, 4438−4444

Table 2. Thermal Properties of the Polymers[a]

sample	T_i/°C	ΔH_i/kJ mol^{-1}	T_g/°C[b]
BB-3(2-Me) homopolymer	172	4.80	64
OH-terminated BB-3(2-Me)-116	171	5.10	64
BB-3(2-Me)-116-85	157	2.41	77
BB-3(2-Me)-116-73	160	3.16	70
BB-3(2-Me)-116-50	165	3.31	69
BB-3(2-Me)-116-42	162	3.50	67
BB-3(2-Me)-116-39	161	3.46	63
BB-3(2-Me)-116-23	164	3.70	65
OH-terminated BB-3(2-Me)-63	159	3.98	60
BB-3(2-Me)-63-68	152	2.94	70
BB-3(2-Me)-63-62	152	3.08	64
BB-3(2-Me)-63-52	158	3.06	70
BB-3(2-Me)-63-45	158	3.21	68
BB-3(2-Me)-63-36	153	3.14	65
BB-3(2-Me)-63-28	147	3.57	60
BB-3(2-Me)-63-16	144	3.58	61

[a]Determined from DSC thermograms measured at a heating rate of 10 °C min^{-1}. [b]The glass transitions of the BB-3(2-Me) and PEMA segments were not identified individually because these segments presented similar T_g values.

WAXS measurements were performed. Figure 2a shows a typical WAXS pattern measured for a fibrous BB-3(2-Me)-116-23 copolymer. The diffraction pattern displays characteristic peaks for the SmCA structure, exhibiting smectic layer reflections on the meridian and the outer halos with a d spacing of 0.45 nm. These reflections spread and display intensity maxima above and below the equator. The smectic layer spacing amounted to 1.38 nm. These features are identical to those of the fibrous BB-3(2-Me) homopolymer,[13] suggesting that in all of the fibrous copolymers the LC segments form the same SmCA structure, in which the backbone is mainly extended along the fiber axis.

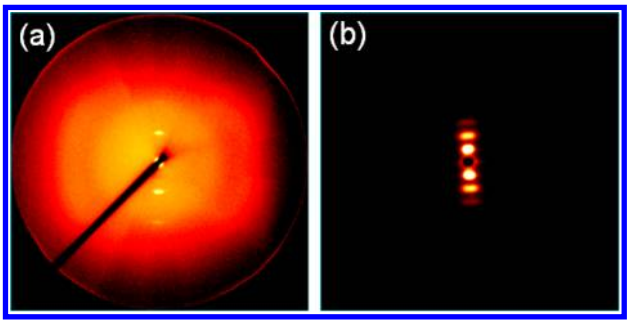

Figure 2. (a) WAXS and (b) SAXS patterns of fibrous BB-3(2-Me)-116-23. The fiber axis is vertical.

3.3. Microdomain Structures. *3.3.1. BB-3(2-Me)-116-φ Copolymers.* The BB-3(2-Me)-116-φ copolymers formed lamellar microdomains for φ < 50%. Figure 2b shows the SAXS pattern of the fibrous BB-3(2-Me)-116-23 copolymer. The pattern presented multiple sharp peaks on the meridian parallel to the fiber axis. The ratios of the scattering vectors (q) equaled 1, 2, and 3 for these peaks, indicating lamellar stacking along the fiber axis direction. Therefore, LC lamellae and smectic layers are parallel to each other. Similar SAXS patterns were observed for all of the copolymers for φ < 50%. Figure 3 shows the scattering intensity averaged over azimuthal sectors of 10° on each side of the meridian as a function of the scattering vector q. Differences in the relative intensities were observed for the block copolymers for peaks of successive order with φ < 50%. Because peak intensities can be associated with the ratios of the lamellar phase thicknesses, d_{LC}, d_{am}, and their standard deviations (σ_{LC} and σ_{am}, respectively) can be estimated by numerically fitting the SAXS profiles using the paracrystal theory.[9,12,14] The parameter values obtained for the best-fit profiles are listed in Table 3. Here d_{am} was assumed to be smaller than d_{LC} because φ < 50%. Also, deviations between the observed and calculated profiles were allowed for the first- and second-order peaks because these peaks at smaller q can be smeared as a result of finite instrumental resolution.

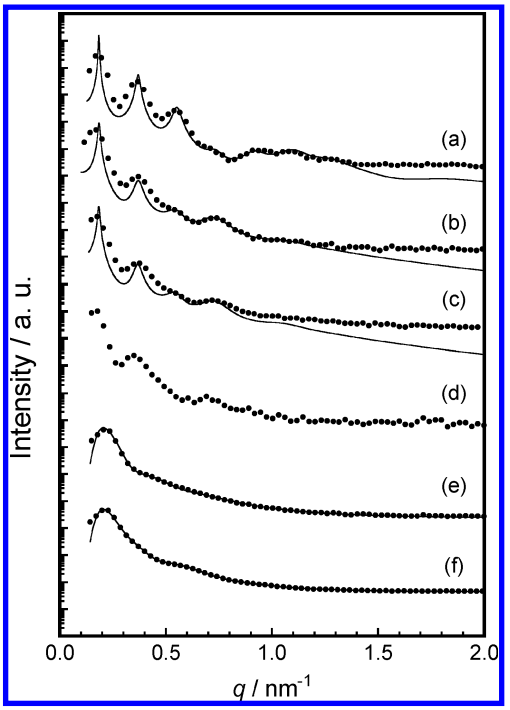

Figure 3. SAXS intensity profiles (dots) for BB-3(2-Me)-116-φ with φ = (a) 23%, (b) 39%, (c) 42%, (d) 50% (e) 73%, and (f) 85%. The solid curves in (a–c) show the intensities calculated using the paracrystal theory, and the curves in (e) and (f) were obtained using the Percus–Yevick hard-sphere structure model.

When φ exceeded 60%, the copolymers formed disordered spherical microdomains. Although the samples could be spun, the resulting fibers shrunk significantly during annealing, and the SAXS patterns became isotropic. The intensity profile of BB-3(2-Me)-116-73 showed a main interference peak at 0.2 nm^{-1} and a sphere form-factor peak, which appeared as a shoulder peak at around 0.4 nm^{-1} (Figure 3e), consistent with the presence of disordered spheres. The interference peak gave an average distance (d_0) of 31 nm between two adjacent LC sphere centers, and the sphere form-factor peak provided an average LC sphere diameter (D_{LC}) of 29 nm. The SAXS intensity profile of BB-3(2-Me)-116-85 exhibited a similar main interference peak at 0.2 nm^{-1}; however, the sphere form-factor peak appeared at a larger scattering vector (q = 0.6 nm^{-1}; Figure 3f). This indicates that an increase in φ from 73% to 85% maintains d_0 but decreases D_{LC} from 29 to 19 nm. Spheres displaying different D_{LC} dispersed at similar d_0 were observed by TEM in copolymer bulk samples (Figure 4). Table 4 lists the D_{LC} values and their standard deviations (σ_D) estimated by numerically fitting the SAXS intensity profile with the Percus–Yevick hard-sphere structure model.[15]

dx.doi.org/10.1021/ma500798z | Macromolecules 2014, 47, 4438–4444

Table 3. Structural Parameters of Lamellar Microdomains Determined by the Paracrystal Theory

sample	d_0/nm	d_{LC}/nm	d_{am}/nm	σ_{LC}/nm	σ_{am}/nm	N_{fold}
BB-3(2-Me)-116-50	35.3	–	–	–	–	–
BB-3(2-Me)-116-42	34.0	20.6	13.4	2.2	2.2	1.7
BB-3(2-Me)-116-39	33.8	20.6	13.2	2.2	2.2	1.7
BB-3(2-Me)-116-23	34.0	26.1	7.9	1.9	0.9	1.1
BB-3(2-Me)-63-52	23.4	–	–	–	–	–
BB-3(2-Me)-63-45	22.6	–	–	–	–	–
BB-3(2-Me)-63-36	22.9	15.8	7.3	1.4	1.1	0.8
BB-3(2-Me)-63-28	22.2	15.8	6.4	1.2	0.9	0.8
BB-3(2-Me)-63-16	23.7	18.7	5.0	1.3	0.9	0.6

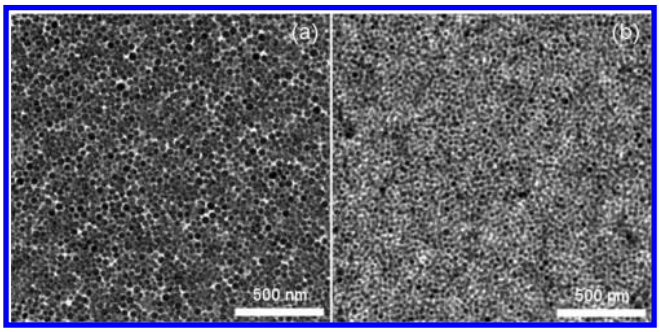

Figure 4. TEM micrographs of (a) BB-3(2-Me)-116-73 and (b) BB-3(2-Me)-116-85. The BB-3(2-Me) domains were stained with RuO_4 vapor to appear black while the PEMA domains are white. The scale bars represent 500 nm.

Table 4. Structural Parameters of Spherical Microdomains Determined Using the Percus–Yevick Hard-Sphere Structure Model

sample	d_0/nm	D_{LC}/nm	σ_D/nm
BB-3(2-Me)-116-85	30.5	17.6	3.2
BB-3(2-Me)-116-73	31.3	23.1	4.5
BB-3(2-Me)-63-68	27.0	20.4	3.6

3.3.2. BB-3(2-Me)-63-φ Copolymers. When $M_{n,LC}$ decreased, the copolymer formed a different microdomain structure. Figure 5 shows the 2D SAXS patterns of BB-3(2-Me)-63-φ copolymers. BB-3(2-Me)-63-16 exhibited scattering maxima on the meridian and was well-connected to the lamellar structure. With increasing φ, the meridional reflections began to split on either side of the meridian and increased the splitting angle. The profiles of the SAXS intensities integrated along the reflection direction displayed several maxima at q with integer ratios (Figure 5). Therefore, for $\varphi < 52\%$, the copolymers formed lamellar microdomains that were tilted with respect to the fiber axis. Also, the tilt angle increased with increasing φ. These lamellae were observed in the fibrous samples by TEM (Figure 5). However, the thickness ratio of the LC domains, which appear as dark stripes, seems larger than that determined by SAXS (see Table 3). The LC lamellae may be swollen by RuO_4, and the interface between the BB-3(2-Me) and PEMA blocks can be diffuse. BB-3(2-Me)-x-φ copolymers exhibit larger values of σ_{am}/d_{am} (ca. 0.15) than those determined for the homologous copolymers with a BB-5(3-Me) segment (ca. 0.08).[9]

SAXS maxima appeared at larger splitting angles for $\varphi = 62\%$ (Figure 5k) and concentrated on the equator for $\varphi = 68\%$ (Figure 5m), while the corresponding WAXS patterns were similar to those recorded at lower φ. The SAXS intensity profiles were different from those acquired for $\varphi < 52\%$, suggesting alterations in the type of microdomain (Figure 6f,g). TEM images presented lamellae with short correlation length and spheres in these fibrous copolymers with $\varphi = 62\%$ and 68%, respectively. The SAXS intensity profile of BB-3(2-Me)-63-68 was well-fitted to the Percus–Yevick hard-sphere structure model, and a sphere diameter of $D_{LC} = 20.4$ nm was obtained (Table 4). In summary, BB-3(2-Me)-63-φ copolymers form lamellar, zigzag lamellar, and disordered spherical microdomains with increasing φ. The zigzag lamellar morphology is a characteristic of copolymers with a short LC segment.

4. DISCUSSION

Models were constructed to show how segment chains are accommodated in lamellar, zigzag lamellar, and spherical microdomains.

4.1. Lamellar Microdomains. BB-3(2-Me)-116-φ copolymers with $\varphi < 50\%$ generated well-ordered lamellar microdomains. A model showing how the copolymer chains pack in the microdomains can be constructed by comparing the SAXS and WAXS patterns as well as d_{LC} and the average contour length l_{LC} of the BB-3(2-Me) segment, respectively. An l_{LC} value of 54 nm was calculated for BB-3(2-Me)-116-φ using $M_{n,LC}$ and the smectic layer spacing. In the SAXS and WAXS patterns, both reflections attributed to stacked lamellae and smectic layers appeared in the fiber axis direction, indicating that the LC segment backbone lies in its most extended conformation along the lamella normal. Therefore, LC segments are most stretched along the lamellar normal direction, although l_{LC} (54 nm) is more than twice as long as d_{LC} (21–26 nm), thus revealing that these segments fold to fit in the lamellae.

Figure 7 shows d_0, d_{LC}, and d_{am} as functions of $M_{n,am}$. d_{am} increases with $M_{n,am}$ according to the relationship $d_{am} \sim M_{n,am}^{0.66}$, which suggests that the dimensions of the PEMA segments are comparable with those of the segments in the amorphous block copolymers ($\sim M^{2/3}$). On the other hand, d_{LC} decreases to counteract the increase in d_{am} by suppressing the increase in d_0. While the amorphous segment enlarges its interface with the LC segment with increasing $M_{n,am}$, the LC segment with a constant molecular weight needs to occupy the same interface area as the amorphous segment to form lamellar microdomains. This condition causes a decrease in d_{LC} with increasing $M_{n,am}$. The LC segment increases the number of folds per chain to enlarge its interface with the PEMA segment (Figure 8a,b). With the assumption of hairpin folding of the LC segment, the average number of folds is increased from 1 to 2 for BB-3(2-Me)-116-φ copolymers [$N_{fold} = (l_{LC}/d_{LC} - 1)$; Table 3].

dx.doi.org/10.1021/ma500798z | Macromolecules 2014, 47, 4438–4444

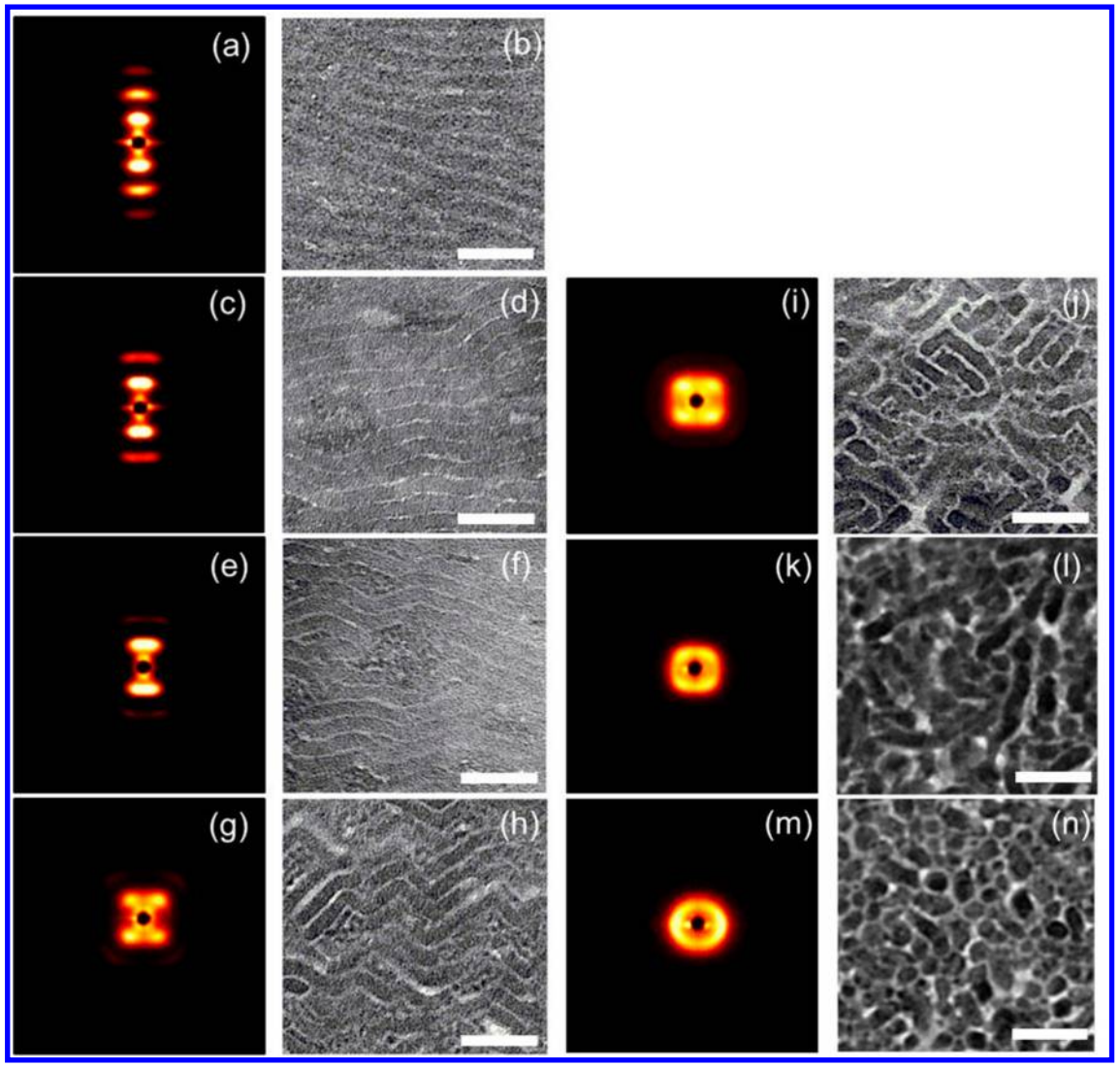

Figure 5. (a, c, e, g, i, k, m) SAXS patterns and (b, d, f, h, j, l, n) TEM micrographs of BB-3(2-Me)-63-φ with φ = (a, b) 16%, (c, d) 28%, (e, f) 36%, (g, h) 45%, (i, j) 52%, (k, l) 62%, and (m, n) 68%. The scale bars in the TEM micrographs represent 100 nm.

A comparison of d_{LC} and N_{fold} values with those measured for similar copolymers containing a BB-5(3-Me) central block shows that the lamella thickness is dependent on the flexibility of the LC segment. Lamellar phases have previously been observed for similar BB-5(3-Me)-100-φ copolymers containing a BB-5(3-Me) polyester central block with $M_{n,LC}$ = 10 000.[9] BB-5(3-Me) polyester bearing a 3-methylpentane spacer is more flexible than BB-3(2-Me) polyester containing a 2-methylpropane spacer. Although the BB-5(3-Me) segment (50 nm) and the BB-3(2-Me)-116 chain (54 nm) displayed comparable l_{LC} values, d_{LC} ranged from 10 to 13 nm for BB-5(3-Me)-100-φ copolymers, which is almost half of that of BB-3(2-Me)-116-φ. This difference between the d_{LC} values for these copolymer series is attributed to the difference in LC segment flexibility for the BB-5(3-Me) and BB-3(2-Me) polyesters. More rigid BB-3(2-Me) segments are folded less frequently than BB-5(3-Me) segments. Thus, the BB-3(2-Me) segment occupies a smaller interfacial area than the BB-5(3-Me) segment, and d_{am} becomes about 1.5 times larger for BB-3(2-Me)-116-φ copolymers (solid symbols in Figure 7) than for BB-5(3-Me)-100-φ copolymers at the same $M_{n,am}$ (open symbols in Figure 7).

4.2. Zigzag Lamella. The BB-3(2-Me)-63-φ copolymers exhibited zigzag lamellar morphologies in which the lamellar normal was tilted with respect to the fiber axis and the chain axis of the BB-3(2-Me) block remained parallel to the fiber axis. Figure 8e depicts a possible chain packing arrangement in the zigzag lamellar structure. The distance between the LC lamellar boundaries along the fiber axis equals $d_{LC}/\cos\alpha$, where α is the angle between the chain axis and the lamellar normal. α can be estimated from the splitting angle of the innermost reflections in the 2D SAXS pattern shown in Figure 5 and increases with increasing φ. The α values amounted to 0°, 9.7°, 11.3°, 36.4°, and 44.5° for the five BB-3(2-Me)-63-φ copolymers with φ increasing from 16% to 52%. The distance between the LC lamellar boundaries along the fiber axis decreased slightly from 19 to 16 nm with increasing φ. These values are almost half of the BB-3(2-Me) segment contour length (l_{LC} = 29 nm), suggesting that once-folded BB-3(2-Me) blocks are accommodated in the LC lamellae. The PEMA segment dimensions increase with increasing $M_{n,am}$, but N_{fold} does not increase. Instead, the LC segments mutually slide along the chain axis to increase the interface between segments. Thus, the LC segments may behave as rigid rods. Similar zigzag lamellar

dx.doi.org/10.1021/ma500798z | Macromolecules 2014, 47, 4438−4444

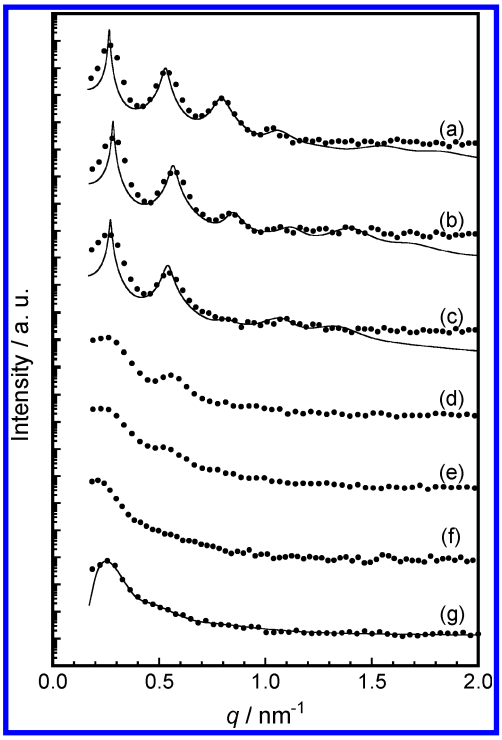

Figure 6. SAXS intensity profiles (dots) of BB-3(2-Me)-63-φ with φ = (a) 16%, (b) 28%, (c) 36%, (d) 45%, (e) 52%, (f) 62%, and (g) 68%. The solid curves in (a–c) show the intensities calculated using the paracrystal theory, and the curve in (g) was obtained using the Percus–Yevick hard-sphere structure model.

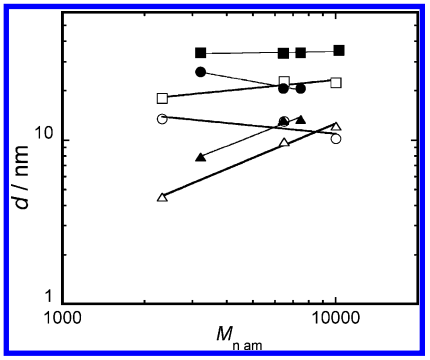

Figure 7. Lamellar spacing (d_0, squares), thickness of LC (d_{LC}, circles), and thickness of amorphous lamellae (d_{am}, triangles) for BB-3(2-Me)-116-φ (solid symbols) and BB-5(3-Me)-100-φ copolymers (open symbols)[9] as functions of the number-average molecular weight of the amorphous segment ($M_{n,am}$). The lines are guides for the eye and have slopes of 0.02, −0.30, and 0.66 for d_0, d_{LC}, and d_{am} of the BB-3(2-Me)-116 copolymers, respectively.

morphologies have been reported for rod–coil block copolymers,[4,5] although simulation studies have suggested that the zigzag lamellar phase is a locally stable structure resulting from collisions of smectic C domains having tilt angles with opposite signs that are grown from randomly-generated nuclei.[16] The polymer chains are hardly folded into stems with lengths less than 16 nm, indicating that the persistence length (l_p) of BB-3(2-Me) chains is about 16 nm.

4.3. Disordered Spheres. The LC segments in copolymers with φ values exceeding 60% were accommodated into spheres and exhibited a smectic layer reflection that was concentrated in the fiber axis direction for the fibrous samples. These facts

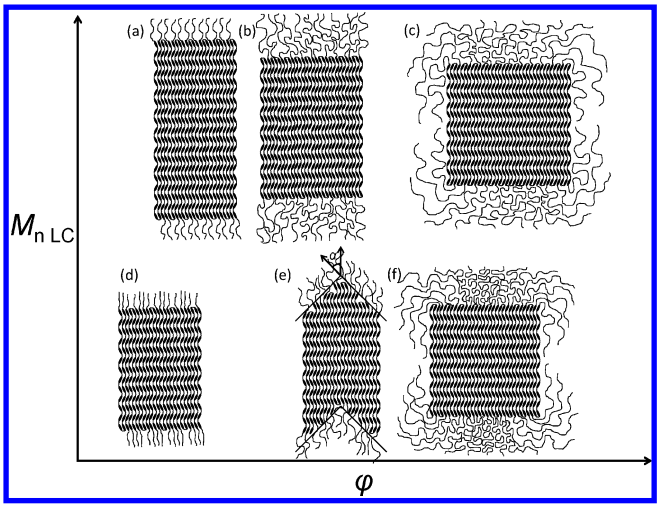

Figure 8. Schematic morphologies of (a) BB-3(2-Me)-116-23, (b) BB-3(2-Me)-116-42, (c) BB-3(2-Me)-116-73, (d) BB-3(2-Me)-63-16, (e) BB-3(2-Me)-63-52, and (f) BB-3(2-Me)-63-68.

indicate that LC segments are most extended to form smectic layers but are folded to fit in the spheres embedded in a PEMA matrix.

Geometric considerations of the lamella-to-sphere morphological change suggest that spheres arise from LC lamellae that are split into cubes. When an LC lamella is divided into cubes with each side measuring d_{LC} to minimize their surface area and these cubes change into spheres to preserve the volume, the sphere diameter (D_{LC}) should be equal to $1.24d_{LC}$. BB-3(2-Me)-116-73 shows a D_{LC} value of 23.1 nm, which is 1.12 times larger than the d_{LC} value of BB-3(2-Me)-116-42. Moreover, BB-3(2-Me)-63-68 presents a D_{LC} value of 20.4 nm, which is 1.29 times larger than the d_{LC} value of BB-3(2-Me)-63-36. These ratios of D_{LC} to d_{LC} are comparable with the expected ratio of 1.24, suggesting that the lamella-to-sphere transition occurs by division of lamellae.

The question arises here as to why the lamella has to be chopped as φ increases up to 60%. In the BB-3(2-Me)-116-φ copolymers, the LC segments can increase the interface by increasing N_{fold} but cannot be folded further when the stem length becomes shorter than 16 nm. If the copolymer maintains a lamellar morphology at higher $M_{n,am}$, the PEMA chain dimensions have to increase only in the lamella normal direction by stretching to generate a high entropy cost. This entropy cost may decrease if LC segments are packed radially into a cylinder or a sphere to increase the PEMA segment dimensions at shorter distances from the interface. However, such a radial packing of LC segments seldom occurs, which contradicts the LC orientational order. Instead, LC lamellae prefer to break into cubes, and PEMA segments emanating from the top and bottom cube surfaces fill the volume near the cube sides to limit stretching in the same way that rod–coil block copolymers can form hockey-puck micelles.[17] Simulations of the self-assembly of semiflexible–flexible block copolymers showed that the semiflexible segments oriented in one direction form disordered sphere microdomains that are immersed in a flexible segment matrix.[18]

In the BB-3(2-Me)-63-φ copolymers, the LC segments fold with a stem length comparable to the persistence length and behave like rods. With increasing φ, such LC segments tilt from the lamellar normal to increase the interfacial area. While this increases the interfacial energy, it decreases the grafting density

dx.doi.org/10.1021/ma500798z | Macromolecules 2014, 47, 4438–4444

of the amorphous chains on the lamellar boundaries, thus increasing the entropy of the amorphous chains. The entropy gain of the limited PEMA chain stretching can compensate for the increment of the interfacial energy.[19,20] The increase in the interfacial energy may exceed the entropy gain when the tilt angle becomes larger than 45°, at which point the lamellae prefer to be divided into cubes. Interestingly, the critical fraction in both cases corresponds to 60%. The lamella-to-sphere transition has been observed for similar block copolymers containing a BB-5(3-Me) central block, and its mechanistic details are now under investigation.

5. CONCLUSIONS

Self-assembled structures of two series of BB-3(2-Me)-*x*-φ copolymers with different $M_{n,LC}$ were investigated. Although the BB-3(2-Me) segments in all of the fibrous copolymers formed smectic layers with the normal along the fiber axis, the type of microdomain depended on φ. While BB-3(2-Me)-*x*-φ copolymers with φ values below 55% formed lamellar microdomains, they accommodated LC segments into spheres embedded in the PEMA matrix for φ values exceeding 68%.

In the lamella microdomains, LC segments were most extended along the lamella normal but folded to fit into the lamellae. When $M_{n,am}$ increased, N_{fold} increased from 1 to 2 for BB-3(2-Me)-116-φ to enlarge the interface with PEMA segments. In contrast, the LC segment of the BB-3(2-Me)-63-φ copolymers folded once but could not be folded further, as otherwise the stem length would become shorter than l_p. Such LC segments formed zigzag lamellae by sliding mutually along the chain axis to increase the interface with the PEMA segments.

With a progressive increase in $M_{n,am}$ to increase φ to more than 55%, the LC segment of BB-3(2-Me)-116-φ cannot increase the interface by increasing N_{fold} because the stem length at N_{fold} = 2 is comparable with l_p. With increasing $M_{n,am}$ at a constant interfacial area, the PEMA segment has to stretch and pay an entropy penalty. To avoid PEMA segment stretching, the LC lamellae break into cubes and PEMA segments emanate from the top and bottom surfaces and fill the volume near the cube sides, hence stretching less. The zigzag lamellae, which are characteristic of BB-3(2-Me)-63-φ, involve interfacial energy that increases with the tilt angle. The increase in the interfacial energy exceeds the conformation entropy gain of PEMA chain at a tilt angle of 45° and triggers the transformation of LC lamellae into spheres. Thus, the lamella-to-sphere transitions in these copolymers are attributed to maximization of the conformational entropy of flexible PEMA segments tethered at the two ends of the semiflexible LC segment.

The flexibility of the central semiflexible segments influences the size of the microdomain. BB-3(2-Me)-116-φ formed lamellar structures with d_{LC} and d_0 larger than those of the copolymers having a BB-5(3-Me) segment with a comparable contour length, indicating that the number of folds increases with an increase in the flexibility of the LC segment. Our results demonstrate that semiflexible−flexible block copolymers can vary their morphology characteristically by the contour length and flexibility of the semiflexible segment in addition to other factors known for flexible copolymers.

AUTHOR INFORMATION

Corresponding Author

*E-mail: mtokita@polymer.titech.ac.jp.

Notes

The authors declare no competing financial interest.

REFERENCES

(1) Bates, C. M.; Maher, M. J.; Janes, D. W.; Ellison, C. J.; Willson, C. G. *Macromolecules* **2014**, *47*, 2−12.
(2) Castelletto, V.; Hamley, I. W. *Curr. Opin. Solid State Mater. Sci.* **2004**, *8*, 426−438.
(3) Olsen, B.; Segalman, R. *Mater. Sci. Eng., R* **2008**, *62*, 37−66.
(4) Chen, J. T.; Thomas, E. L.; Ober, C. K.; Hwang, S. S. *Macromolecules* **1995**, *28*, 1688−1697.
(5) Chen, J. T.; Thomas, E. L.; Ober, C. K.; Mao, G.-p. *Science* **1996**, *273*, 343−346.
(6) Tenneti, K. K.; Chen, X.; Li, C. Y.; Tu, Y.; Wan, X.; Zhou, Q.-F.; Sics, I.; Hsiao, B. S. *J. Am. Chem. Soc.* **2005**, *127*, 15481−15490.
(7) Radzilowski, L. H.; Stupp, S. I. *Macromolecules* **1994**, *27*, 7747−7753.
(8) Radzilowski, L. H.; Carragher, B. O.; Stupp, S. I. *Macromolecules* **1997**, *30*, 2110−2119.
(9) Koga, M.; Ishige, R.; Sato, K.; Ishii, T.; Kang, S.; Sakajiri, K.; Watanabe, J.; Tokita, M. *Macromolecules* **2012**, *45*, 9383−9390.
(10) Ishige, R.; Ishii, T.; Tokita, M.; Koga, M.; Kang, S.; Watanabe, J. *Macromolecules* **2011**, *44*, 4586−4588.
(11) Sato, K.; Koga, M.; Kang, S.; Sakajiri, K.; Watanabe, J.; Tokita, M. *Macromol. Chem. Phys.* **2013**, *214*, 1089−1093.
(12) Koga, M.; Sato, K.; Kang, S.; Sakajiri, K.; Watanabe, J.; Tokita, M. *Macromol. Chem. Phys.* **2013**, *214*, 2295−2300.
(13) Fernández-Blázquez, J. P.; Bello, A.; Pérez, E. *Macromol. Chem. Phys.* **2007**, *208*, 2611−2620.
(14) Roe, R.-J. *Methods of X-ray and Neutron Scattering in Polymer Science*; Oxford University Press: New York, 2000.
(15) Kinning, D. J.; Thomas, E. L. *Macromolecules* **1984**, *17*, 1712−1718.
(16) Pryamitsyn, V.; Ganesan, V. *J. Chem. Phys.* **2004**, *120*, 5824−5838.
(17) Williams, D. R. M.; Fredrickson, G. H. *Macromolecules* **1992**, *25*, 3561−3568.
(18) Kumar, N. A.; Ganesan, V. *J. Chem. Phys.* **2012**, *136*, 101101.
(19) Halperin, A. *Europhys. Lett.* **1989**, *10*, 549−553.
(20) Halperin, A. *Macromolecules* **1990**, *23*, 2724−2731.